

Thermal effect on dynamic performance of high-speed maglev train/guideway system

Long Zhang^{1a} and JingYu Huang^{*1,2}

¹College of Civil Engineering, Tongji University, Shanghai 200092, China

²National Maglev Transportation Engineering R&D Center, Tongji University, Shanghai 201804, China

(Received May 17, 2018, Revised September 20, 2018, Accepted October 11, 2018)

Abstract. Temperature fields and temperature deformations induced by time-varying solar radiation, shadow, and heat exchange are of great importance for the ride safety and quality of the maglev system. Accurate evaluations of their effects on the dynamic performances are necessary to avoid unexpected loss of service performance. This paper presents a numerical approach to determine temperature effects on the maglev train/guideway interaction system. Heat flux density and heat transfer coefficient of different components of a 25 m simply supported concrete guideway on Shanghai High-speed Maglev Commercial Operation Line is calculated, and an appropriate section mesh is used to consider the time-varying shadow on guideway surfaces. Based on the heat-stress coupled technology, temperature distributions and deformation fields of the guideway are then computed via Finite Element method. Combining guideway irregularities and thermal deformations as the external excitations, a numerical maglev train/guideway interaction model is proposed to analyze the temperature effect. The responses comparison including and excluding temperature effect indicates that the temperature deformation plays an important role in amplifying the response of a running maglev, and the parameter analysis results suggest that climatic and environmental factors significantly affect the temperature effects on the coupled maglev system.

Keywords: high-speed maglev transport; maglev train/guideway interaction system; thermal analysis; temperature effect; dynamic performance

1. Introduction

The Maglev transport is a highly modern transportation mode, which has the merits of wear-free, higher running speed, lower energy consumption, lower noise emission and less maintenance requirement than the traditional railway transportation. When the maglev train moves along guideways, the complicate maglev train/guideway interaction occurs. If excessive vibrations or resonance happen between the train and guideway, it may cause a suspension instability or bad ride quality for maglev vehicle (Kim *et al.* 2015). Therefore, the dynamic performances of the train and guideway become an important research issue for the maglev system.

In the past few decades, many scholars have studied the dynamic problem of the maglev train/guideway system. Various numerical models including simplified two-dimensional models (Cai *et al.* 1994, Cai and Chen 1996, Kong *et al.* 2011, Lee *et al.* 2009, Min *et al.* 2012, Yau 2009a, 2010a, Zhang and Huang 2018) and complicated three-dimensional models (Han *et al.* 2016, Kim *et al.* 2015, Min *et al.* 2017a, Shi and Wang 2011, Song and Fujino 2008) with various electromagnetic force controllers have

been proposed to simulate the coupled system and to analyze their dynamic responses under diverse external excitation conditions. In these excitation situations, the wavelength of guideway surface irregularities has great influence on the maglev system vibration, which has been investigated by the most previous studies. Zhao and Zhai (2002), Shi *et al.* (2007), Ren *et al.* (2010), Talukdar and Talukdar (2016) and Huang *et al.* (2018) used the power spectral density function (PSD) to describe the random guideway surface irregularity, and the effect of irregularity on the coupled system responses and ride quality of maglev vehicles were carefully studied by these work. Wind is one of the most influential excitations for the ride quality of the maglev vehicle. Yau (2010b) simulated the aerodynamic forces acting on the moving vehicles as quasi-steady oncoming wind loads with incident turbulent airflow to conduct an investigation on the responses of maglev system. Min *et al.* (2017b) used the spectral process method to simulate the time histories of stochastic wind forces and analyzed the wind effect on the ride quality of the maglev vehicle. These studies indicated that the wind load or aerodynamics forces played an important role in amplifying the response of a running maglev vehicle especially with higher moving speeds. Foundation settlements or occasional earthquakes also are the important excitations for the maglev system. The bridge system is the most generally used structure type for the maglev guideways, thus maglev trains may have to cross areas with foundation settlements or occasional earthquakes. Yau carried out a series of dynamic investigations of maglev trains traveling over

*Corresponding author, Professor
E-mail: huangjingyu@tongji.edu.cn

^aPh.D. Student
E-mail: 88zhanglong@tongji.edu.cn

flexible guideways on the influence of ground settlement (Yau 2009b), horizontal earthquake-induced vibration (Yau 2010c), wave passage effects (Yau 2013), and dynamic interaction of vehicle-guideway system with soil-foundation (Yang and Yau 2011). Numerical results revealed that ground settlements, wave propagation and motion might significantly affect the dynamic responses of the vehicle/guideway interaction system, especially for regions with soft soil deposits. Ju *et al.* (2014) evaluated the safety of a series of maglev trains moving on multi-span bridges subjected to foundation settlements and earthquakes.

Based on the above references, it can be concluded that, so far, the dynamic responses of the maglev system undergoing various external excitation conditions, such as the irregularity, aerodynamic forces, foundation settlements and seismic forces, have been investigated by the previous research. However, rather limited research works have been conducted on the dynamic responses of the maglev system subjected to the thermal effects.

Due to the long-term outside exposure, bridge structures may suffer from stress concentration, local failure, and even integral destruction, which reduce their service performance (Liu *et al.* 2012, Tian *et al.* 2017). Since the levitation gaps between levitation magnets of maglev vehicle and guideway are restrained around 8-10 mm (Zhao and Zhai 2002), the dynamic performances of the high-speed maglev system are sensitive against the change of levitation gap. The climatic and environmental factors may cause thermal deformation of guideway structure, and then induce a variation of the levitation gap and affect the responses of maglev system. If the effect of temperature on the maglev system is not clearly estimated, there is a potential risk of losses of ride safety and quality. The engineering practices on Shanghai High-speed Commercial Operation Line (Wu and Huang 2004) and Test facility TVE in Emsland (MANGERIG *et al.* 2005) also reveal that thermal effect due to climatic influences is an important issue for the construction. Experimental measurement can be applied to collect the data of temperature distribution and deformation, but it will increase the cost of the design and research and cannot evaluate the temperature influence on dynamic responses. Therefore, it is considerably necessary to develop a reliable analysis and calculation method to evaluate the thermal effect on the dynamic responses for the maglev system.

This paper aims to quantify temperature effect on vibration performances of high-speed maglev train/guideway interaction system. First, a thermal analysis is proposed to calculate the temperature field and deformation field of a 24-m simply supported concrete guideway with the consideration of the time-varying solar radiation, shadows, heat convection, and heat transfer between guideway surfaces and the ambient environment. Afterward, a numerical maglev train/guideway interaction model with a feedback current controller is developed, in which the guideway irregularity and the thermal deformations are included as the external excitations. The effects of thermal deformations on the dynamic responses of the maglev system are carefully investigated by the comparison including and excluding the temperature

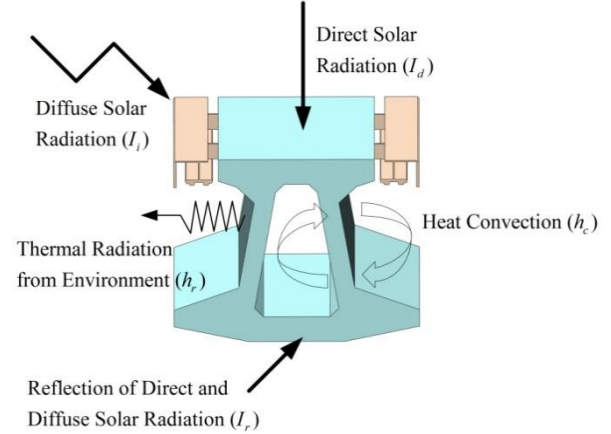


Fig. 1 Heat exchange of guideway under solar radiation

influences. Furthermore, a parametric analysis is conducted to analyze the effects of various parameters, including train speeds, material properties, and climatic conditions, on the dynamic performances of the maglev train/guideway system.

2. Equations of heat conduction and boundary condition

The temperature distribution of the guideway structure is affected by (1) heat transfer by conduction within the material, (2) heat generated within the material, e.g. by hydration, (3) heat transfer at the surface of the guideway by convection, (3) heat flux on boundary of the element due to radiation, including irradiation of solar energy. Under the condition of solar radiation with low wind speed, three ways of heat exchange between the guideway and the environment are shown in Fig. 1. These heat transfer forms are now considered in more detail as follows.

2.1 Conduction heat transfer

Heat transfer by conduction without the heat generated within the structure is governed by Fourier's equation

$$k\left(\frac{\partial^2 T}{\partial x^2} + \frac{\partial^2 T}{\partial y^2} + \frac{\partial^2 T}{\partial z^2}\right) = \rho c \frac{\partial T}{\partial t} \quad (1)$$

in which T = temperature of the guideway ($^{\circ}\text{C}$), k = isotropic thermal conductivity coefficient of units ($\text{W}/(\text{m}\cdot^{\circ}\text{C})$), c = specific heat capacity ($\text{J}/(\text{kg}\cdot^{\circ}\text{C})$), ρ = the density of concrete (kg/m^3).

2.2 Convection heat transfer

The rate of heat transfer by convection is related to the temperature difference between the surface temperature T_s , and the air temperature T_a , the convective heat exchange follows Newton's law

$$q_c = h_c(T_s - T_a) \quad (2)$$

in which h_c = convection heat transfer coefficient ($\text{W}/(\text{m}^2 \cdot ^\circ\text{C})$). The coefficient of h_c , which is related to many variables such as the surrounding wind speed, surface roughness of guideway, material type, and geometric configuration of the exposed structure, is generally determined by experiments or empirical equations. According to some references (Mamdouh and Amin 1984, Walter *et al.* 1983), the values adopted for the convection heat-transfer coefficient h_c at different surfaces can be given as

- (1) Top surface of concrete guideway = $3.83v+4.67$
- (2) Bottom surface of cantilever = $3.83v+2.17$
- (3) Surfaces of guideway inside box = 3.5
- (4) Outside box surface = $3.83v+3.67$

2.3 Radiation heat transfer

The heat transfer between the guideway surface and the surrounding atmosphere due to long wave radiation, i.e., thermal irradiation, produces a nonlinear boundary condition which can be modeled by Stefan-Boltzman radiation law as

$$q_r = C_s e (T_s^4 - T_a^4) \quad (3)$$

in which C_s = Stefan-Boltzman constant = $5.677 \times 10^{-8} \text{ W}/(\text{m}^2 \cdot \text{K}^4)$, e = emissivity coefficient relating the radiation of the guideway surface (a gray body) to that of an ideal black body ($0 \leq e \leq 1$). For convenience, the Eq. (3) can be rewritten in the quasi-linear form of the convection heat transfer

$$q_r = h_r (T_s - T_a) \quad (4)$$

in which h_r ($\text{W}/(\text{m}^2 \cdot ^\circ\text{C})$) is a radiation heat transfer coefficient defined as (Branco *et al.* 1991, 1992)

$$h_r = e(4.8 + 0.075(T_a - 5)) \quad (5)$$

Once the radiation coefficient h_r is calculated, it can be treated similarly to the convection coefficient h_c , and the effects of heat convection and heat radiation can thus be combined in an overall heat transfer coefficient h

$$h = h_r + h_c \quad (6)$$

2.4 Solar radiation on a surface

The solar radiation is the major source of radiation energy to heat up the guideway structure. According to the acting way, the solar radiation includes three parts, including the direct solar radiation I_d , diffuse solar radiation I_i , and reflection of direct and diffuse solar radiation I_r . Based on the empirical equations of references (Branco *et al.* 1992, Walter *et al.* 1983), these radiations intensity values (I_d , I_i , I_r) can be calculated with the solar constant I_0 and the environmental factors in the atmosphere. Alternatively, the intensity values can be experimental determined by thermal measurements.

The solar radiation intensity on a surface of a box

guideway is related to various angles between solar beam and the plane of the guideway. The direct solar radiation I_d on a plane of arbitrary orientation (e.g., the sides of a box girder) depends upon the incident angle, θ , between the incoming solar beam and the surface angle, and the diffuse solar radiation I_i and reflection of direct and diffuse solar radiation I_r depend upon the angle, β , between the horizontal and the surface. The overall solar radiation I on the side of arbitrary orientation of a box guideway can be expressed as

$$I = I_d \cos \theta + I_i \cos^2 \frac{\beta}{2} + I_r \sin^2 \frac{\beta}{2}, \quad I' = \varepsilon I \quad (7)$$

in which $\varepsilon = 0.65$ is the solar radiation absorptivity of concrete guideways, I' is the solar radiation after absorption, the incident angle θ can be described in terms of several other angles as (Mamdouh and Amin 1984, Walter *et al.* 1983)

$$\begin{aligned} \cos \theta = & \sin \delta \sin \phi \cos \beta - \sin \delta \cos \phi \sin \beta \cos \gamma \\ & + \cos \delta \cos \phi \cos \beta \cos \tau + \cos \delta \sin \phi \sin \beta \cos \gamma \cos \tau \\ & + \cos \delta \sin \beta \sin \gamma \cos \tau \end{aligned} \quad (8)$$

in which ϕ = latitude of the location (north positive), δ = solar declination, i.e., the angular position of the sun at solar noon with respect to the plane of the equator (north positive), γ = surface azimuth angle, i.e., the angle between the normal to the surface and the local meridian, the zero point being due south, east positive and west negative, and τ = hour angle, solar noon being zero, and each hour equaling 15° of longitude with mornings positive and afternoons negative. The declination δ can be found by the approximation

$$\delta = 23.45 \sin(360 \frac{284 + D}{365}) \quad (9)$$

The solar radiation zone on a surface of a box guideway is affected by several angles and the length of the overhanging cantilever slab ℓ_k . The height of the shade, where no direct beam radiation is present, is given by (Mamdouh and Amin 1984, Walter *et al.* 1983)

$$\ell_s = \ell_k \frac{\tan h}{\sin(90 + \gamma - \tau) \sin \beta - \cos \beta \tan h} \quad (10)$$

in which h = solar altitude, and it can be expressed by

$$\sin h = \sin L \sin \delta + \cos L \cos \delta \cos \tau \quad (11)$$

3. Numerical model of thermal analysis for a maglev guideway

To investigate the temperature and deformation field in a maglev guideway structure, a numerical model of thermal analysis is established, in which thermal boundary conditions, including convection heat transfer, radiation heat transfer, solar radiation, and shadow, are simulated.

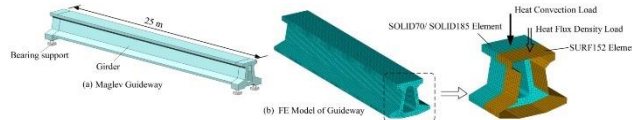


Fig. 2(a) Maglev guideway (b) FE model of the guideway

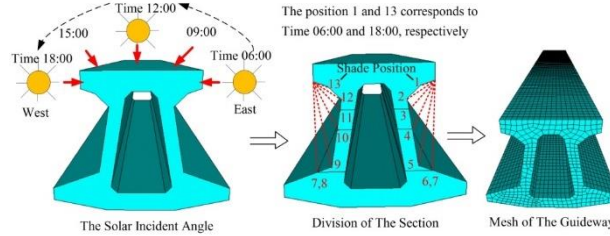
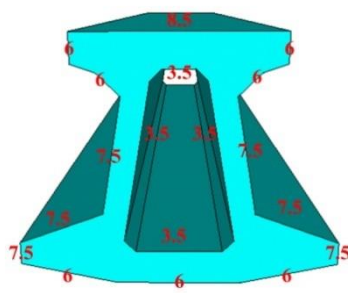
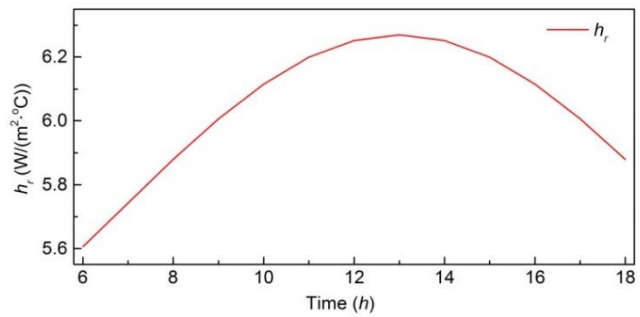


Fig. 3 The solar incident angle, shade region, and the mesh of the guideway

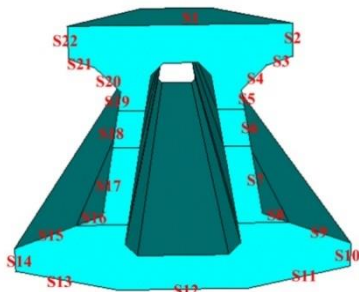


(a)

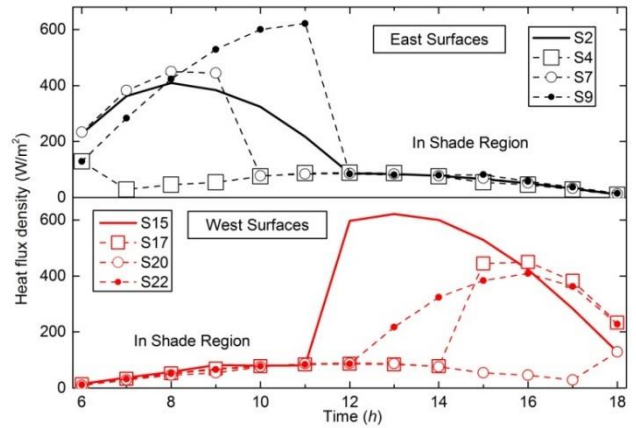


(b)

Fig. 4(a) The thermal convection coefficient (h_c) and (b) the time-varying thermal radiation coefficient (h_r)



(a)



(b)

Fig. 5(a) The division of the outside guideway surface and (b) the heat flux density (I) of guideway surface parts

The 25 m simply supported reinforced concrete (RC) guideway with box section in Shanghai High-speed Maglev Commercial Line, as shown in Fig. 2, is taken as an example for the analysis presented in the article. The real heat exchange between a guideway and its surrounding environment is rather complicated, which is not only affected by complex meteorological conditions but also by conditions specific to the guideway's location, adjacent terrain, and other factors. Although it is difficult to precisely simulate the real and entire thermal process, it is able to focus on the extreme case that the extreme meteorological condition causes a maximum temperature load for a guideway structure. The extreme situation is

Table 1 Main materials properties of the concrete guideway

Parameters	Unit	Value
Young's modulus (E_x)	Pa	5.5×10^{10}
Density (ρ)	kg/m^3	2500
Poisson's ratio		0.3
Thermal conductivity (k)	$W/(m \cdot ^\circ C)$	2.34
Specific heat (C)	$J/(kg \cdot ^\circ C)$	1046
Thermal expansion coefficient (α_T)	$m/^\circ C$	1.18×10^{-5}

defined by the following assumptions and simplifications. (1) Sunny days in July with low wind speed are selected as

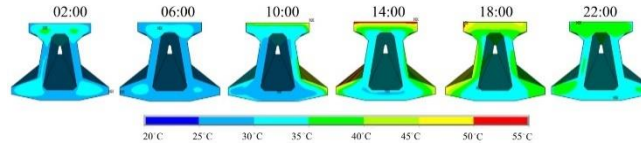


Fig. 6 Temperature distribution variations of guideway surfaces at time 02:00 to time 22:00 of a day

Table 2 The solar intensity of Shanghai in July

Solar Radiation (W/m ²)	Day Time <i>t</i> (h)												
	6	7	8	9	10	11	12	13	14	15	16	17	18
Direct Radiation (<i>I_d</i>)	357	562	681	740	814	847	853	847	814	740	681	562	357
Diffuse Radiation (<i>I_i</i>)	23	57	90	127	123	124	129	124	123	127	90	57	23
Reflection Radiation (<i>I_r</i>)	13	43	68	77	115	136	137	136	115	77	68	43	13

the typical condition to perform the subsequent temperature analysis, (2) The extreme temperature load resulting from complete solar exposure in one day is considered for the concrete guideway, (3) A east-west oriented guideway (the azimuth angle $\gamma = 0^\circ$) is assumed for thermal investigation, because when the guideway span is arranged exactly along a south-north line the maximum temperature difference will occur and the temperature on the sunward side increases much faster than it does in the shaded region (Tian *et al.* 2017), (4) The initial temperature of the guideway is assumed to be uniformly distributed and is the same with the initial surrounding air temperature. The temperature analysis program runs for 72 h, three 24-h cycling periods, to eliminate the errors generated by the initial temperature assumption, (5) The heat generated within the material, for example by hydration, is not considered.

In addition, the concrete material of the guideway is assumed to be homogeneous and elastically isotropic, and its material properties, such as thermal conductivity, specific heat, radiation rate, and density, do not change with temperature. The effect of reinforcement inside the structure on the thermal analysis is ignored. Moreover, it is assumed that the heat transfer and structural deformation do not influence each other continuously, then the temperature field and temperature stress can be calculated as two independent issues.

3.1 FEM model

The temperature and displacement of the guideway here are computed by finite element method using the commercial FE software ANSYS. Three-dimensional (3D) guideway model are established, and complicated thermal boundary conditions, including convection heat transfer and solar radiation, are considered. Fig. 2 shows the FE model of the guideway, in which the girder is modeled by the 3D thermal element of SOLID70 for a temperature analysis and by the corresponding equivalent 3D structural element of SOLID185 for a thermal deformation analysis. The SURF152 elements, which are overlaid onto the outside face of the guideway, are applied to simulate the complicated thermal boundary condition. To avoid the interference between various thermal loads when they are

applied on the same surface of the guideway, the heat convection loads related to the heat convection and heat radiation are applied on the structural outside surface of SOLID70 element, while the heat flux density loads related with solar radiation are applied on the SURF152 element. The mesh of the guideway model not only considers the accuracy and efficiency of simulation, but also considers the effect of time-varying shade region of solar radiation. As shown in Fig. 3, after the computation of the heights of shade regions at different times by Eq. (10) the section of the guideway is divided by the corresponding shade positions. The mesh dimensions for the guideway model in three directions are all controlled to be 0.1 m, which is proved to be refined enough to conduct an accurate thermal and structural analysis. The calculated material parameters are shown in Table 1, which are mainly from the design and research materials of the guideway of Shanghai High-Speed Maglev Commercial Line.

As mentioned above, the thermal boundary condition varies with the position of the point considered on the surface and the time. Therefore, a transient temperature field analysis is conducted to analyze the temperature effect on the guideway structure for 72 h or three 24-h cycling periods, and a time increment Δt of 1.0 hr is used.

3.2 Thermal boundary conditions

The conduction heat transfer at the surface of the guideway is calculated by Eq. (2). In this situation, with the wind speed assumed to be 1 m/s, the conduction heat transfer coefficients h_c for the outside and insider guideway surfaces are obtained in Fig. 4. The radiation heat transfer between the guideway surface and the surrounding atmosphere, which varies with the variable of the air temperature T_a , is calculated by Eq. (4). The air temperature $T_a(t)$ is a function of the time of day, and it is customary that the diurnal air temperature can be assumed as a sinusoidal variation between the minimum temperature $\min T_a$, assumed to occur at 2:00 hr and the maximum value $\max T_a$, assumed to occur at 14:00 hr. With these assumptions, the temperature at any hour, t , of the day can be expressed by (Walter *et al.* 1983)

$$T_a(t) = \frac{1}{2}(\max T_a + \min T_a) + \frac{1}{2}(\max T_a - \min T_a) \times \sin\left[(t - 8) \frac{\pi}{12}\right] \quad (12)$$

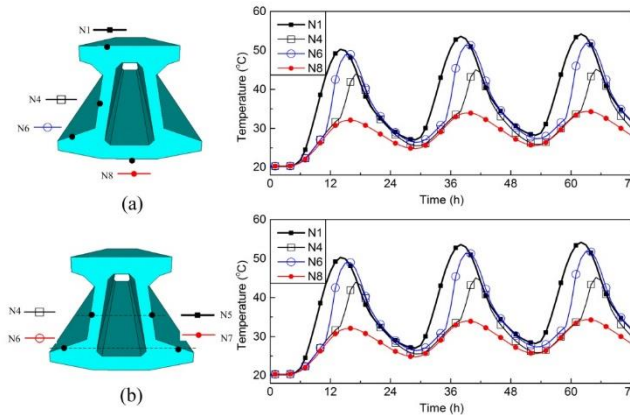


Fig. 7 Temperature time histories at the selected locations

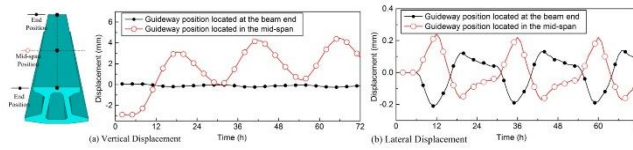


Fig. 8 Displacement time histories at the selected locations

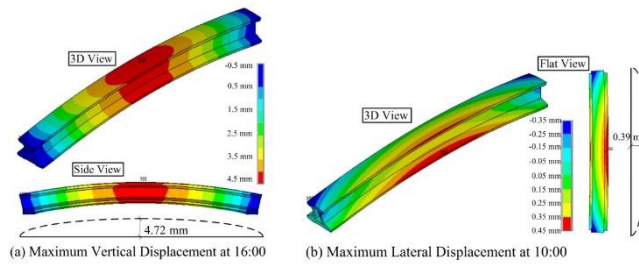


Fig. 9 Vertical and lateral displacement distribution of guideway at time 16:00 and 10:00, respectively

In this study, $\max T_a = 36^\circ\text{C}$ and $\min T_a = 20^\circ\text{C}$ based on the Shanghai meteorological data in July. Fig. 4 shows the radiation heat transfer coefficients h_r for all the guideway surfaces. Therefore, the overall heat transfer coefficient h , including heat convection and heat radiation, can be then obtained by their combination with the Eq. (6). These coefficients are all applied on the SURF152 element.

The effect of solar radiation on the surfaces of the guideway is considered as the heat flux density applied on the outside and inside surface nodes of the guideway structure. The heat flux density of each surface, which varies with the solar incident angle and the shade region, is determined as follows. First, the solar incident angle θ is calculated by Eq. (8) according to the angle parameters, which are given as $\phi = 31.2^\circ$, $\delta = 20.87^\circ$. Then, according to the shade positions at different time t of day shown in Fig. 3, the outside surfaces of the guideway are divided into 22 parts (shown in Fig. 5). The heat flux value of each part is computed by Eq. (7), and it should be noted that the direct solar radiation I_d is zero when the surface part is in the shade region. The intensity values of direct solar radiation, diffuse solar radiation, and reflection of direct and diffuse solar radiation (I_d, I_i, I_r) adopted in this case is listed in Table 2. Using these intensity values, the overall heat flux values I of all the parts can be obtained (shown in Fig. 5). The calculated heat flux density values in the horizontal

plane and four vertical planes by this approach perfectly coincide those of “Thermal Design Code for Civil Building” (GB 50176-93), which indicates that the heat flux intensity value (I_d, I_i, I_r) adopted here can reasonably simulate the solar radiation of the guideway in Shanghai.

3.3 Temperature field and displacement field under extreme temperature condition

Fig. 6 shows the variations in temperature distribution of the guideway at 02:00 to 22:00 of the third 24-h period. It can be observed that the change of temperature varies with the variable of solar radiation incident angle, in which the temperature rises first at the east side of the guideway, then at the top surface, and finally, at the west side of the guideway. Significant temperature change and higher temperature mainly occur on the upper and external regions of the guideway structure, because the solar radiation is less or none in the internal and lower regions and it takes much time to transfer heats from outside and upper regions to these regions with the concrete material. With the increase in the thickness of the components, the temperature change slows down, and for the internal surface of the guideway, the temperature during the entire day maintains below 40°C .

The temperature distribution can be further illustrated by

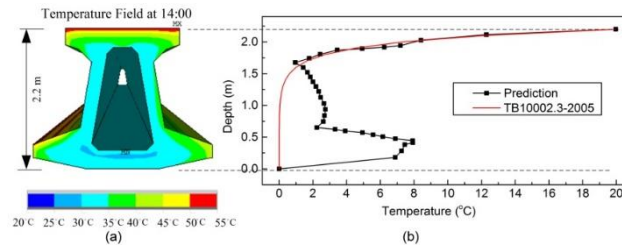


Fig. 10(a) Temperature distribution at time 14:00 (b) Comparison of temperature gradients between the prediction and the design code (TB10002.3-2005)

Fig. 7, in which the temperature variations of the selected locations are plotted with the variation of time. The influence of depth of section, as well as the effect of partial shadows, can be observed by the temperature comparison between the outside surfaces in Fig. 7(a). Because the top surface (N1) is most exposed to solar radiation, its temperature is higher than the other surfaces. The temperature of the outside surface (N4) of the web is significantly affected by the shadows since the upper flange plate blocks direct solar radiation toward the web. Without the direct solar radiation, the temperature of bottom surface is the lowest. Fig. 7(b) presents the temperature differences between the east side and west side. It can be found that the peak temperature values and peak time are significantly affected by the locations of the guideway. To sum up, temperature gradients vary among locations of the guideway and time of the day. In this study, it is obvious that the temperature will influence considerably the guideway deformation, which will be investigated in the following work.

Fig. 7 plots three 24-h period temperature results. The temperature variations at the second and third 24-h periods are observed almost the same, whereas the maximum temperature at the first 24-h is lower than that of other periods. This reveals that an error will be induced when the initial uniform temperature distribution is assumed for the simulation and this error can be almost eliminated after running the program for a continuous cycling period of 24 h. It also indicates that an appropriate assumption of the guideway initial uniform temperature is of great importance for the numerical study.

Temperature effect analysis on structure generally includes investigation of structural deformation and stress field. This paper focused on the service performance of maglev train-guideway system, therefore, only the displacement field is considered for thermal analysis. The vertical and lateral displacement curves at representative points throughout the entire process are presented in Fig. 8. It should be noted that the initial displacement results at the first 24-h cycling period exhibit obvious error with that of the second and third 24-h periods, which emphasizes the importance of appropriate assumption of initial temperature distribution for the guideway structure. The most dangerous situation, i.e., the extreme deformation of the guideway, is defined as the occurrence that the maximum displacement difference between the positions located in mid-span and that at the beam end. This extreme situation can be identified at 16:00 for vertical deformation and 10:00 for

lateral deformation, in which the differences of the vertical and lateral displacement reach their maximum values. Fig. 9 shows the vertical displacement and strain fields of the guideway at 16:00, and the lateral displacement and strain fields of the guideway at 10:00.

A thermal measurement of maglev guideways was performed on testing facility in Emsland/Germany, and the time-varying temperature distribution of the guideway were presented in the reference (MANGERIG *et al.* 2005). By comparison, reasonable agreements in the results of temperature distribution are found between the numerical prediction in this study and the measurement in the reference, which to some extent enables a verification of the accuracy or validity of the numerical prediction.

The temperature gradients at time 14:00 under extreme temperature condition are plotted along the cross sections in Fig. 10. The temperature values are normalized by subtracting the minimum values from the absolute ones. In addition, because the guideway case is assumed to be located at the Shanghai High-speed Maglev Commercial Operation Line, China, then the temperature gradients, specified for concrete railway bridge in this region from the code (TB10002.3-2005), are also plotted in Fig. 10(b) for a comparison. Significant differences of temperature gradients are found in the areas of web and lower flange between the prediction and TB10002.3-2005 code, which are mainly due to the particular section shape of the maglev guideway. The temperatures on the web and upper surfaces of the lower flange have apparent gradients, and that, to a large extent, is attributed to the influences of the solar radiation because the surfaces of the web and lower flange are not totally covered by the upper overhanging slab. Therefore, the design of maglev guideway structure particularly requires a thorough consideration of the complicated section shape and partial shadow coverage effects.

4. Maglev vehicle/guideway interaction model

A maglev train/guideway interaction model is composed of a maglev train subsystem which ignored elastic deformations during vibration and a guideway subsystem established by FE method. These subsystems interact with each other by an electromagnetic interaction force which was tuned by an active current controller. Based on the aforementioned thermal analysis, the vertical displacement value under extreme situation is far larger than the lateral

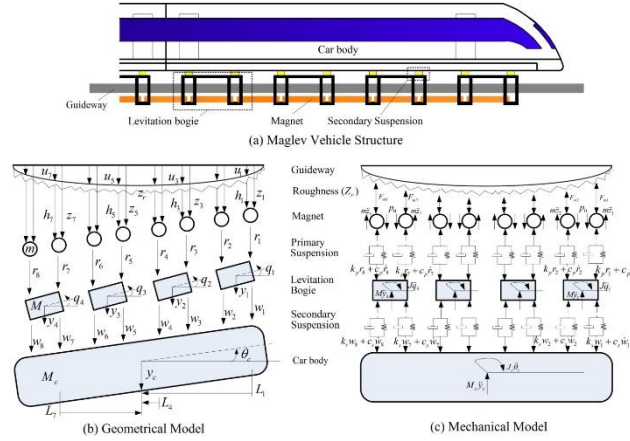


Fig. 11(a) TR08 high-speed maglev vehicle (b) geometrical model (c) mechanical model of the vehicle

one. Moreover, the vertical vibration dominates the dynamic behavior of the maglev vehicle/guideway interaction (Yau 2009a). Therefore, only the vertical temperature deformation and its effect on vertical vibration are considered here.

4.1 Maglev train subsystem

In this study, the maglev train subsystem contains many vehicles, which are based on the structure of Transrapid08 (TR08) high-speed maglev vehicle (shown in Fig. 11). Each maglev vehicle consists of one car body, four levitation bogies, eight magnets and spring-damper suspensions. Every car body or bogie has two DOFs (one translational and one rotational displacement), and they connect with each other by two spring-dampers (k_s and c_s) which form the secondary suspension. y_n , q_n denote the vertical and rotational displacements of the n th levitation bogie, and y_c , θ_c denote that of the car body. Every magnet has one translational DOF (z_n for n th magnet), and two magnets as a group connect one bogie by two spring-dampers (k_p and c_p) which form the primary suspension. Each magnet interacts with the guideway by the electromagnetic force (F_{mn} for the n th magnet), which is tuned by an active current controller. Thus, every maglev vehicle has 18 DOFs for the vertical vibration. Fig. 11 shows the geometrical and mechanical models of the maglev vehicle structure. The dynamic equation of the n th magnet can be expressed as

$$m\ddot{z}_n + c_p\dot{r}_n + k_p r_n = p_0 - F_{mn}, \quad n = 1, 2, \dots, 8 \quad (13)$$

where m is the mass of the magnet, $p_0 = (m + M/2 + M_c/8)g$ is the static load for the magnet, M is the mass of the levitation bogie and M_c is the mass of the car body, r_n is the relative displacement between the n th magnet and the corresponding e th levitation bogie, which is given by

$$r_n = z_n - y_{ve} = z_n - (y_e + (-1)^n L_0 \theta_e) \quad (14)$$

where L_0 is half length of the levitation bogie, y_e and θ_e are the displacements of the levitation bogie which relates to the n th magnet. The relationship between e and n can be seen in Fig. 11(b).

The dynamic equilibrium equation of the e th levitation bogie can be written as ($e = 1, 2, 3, 4$)

$$\begin{cases} M\ddot{y}_e + (k_s w_n + c_s \dot{w}_n - k_p r_n - c_p \dot{r}_n) + \\ (k_s w_{n+1} + c_s \dot{w}_{n+1} - k_p r_{n+1} - c_p \dot{r}_{n+1}) = 0 \\ J\ddot{q}_e + (k_s w_n + c_s \dot{w}_n - k_p r_n - c_p \dot{r}_n)(-1)^n L_0 + \\ (k_s w_{n+1} + c_s \dot{w}_{n+1} - k_p r_{n+1} - c_p \dot{r}_{n+1})(-1)^{n+1} L_0 = 0 \end{cases} \quad (15)$$

where J is the moment of inertia of the levitation bogie, w_n and w_{n+1} are the relative displacements between the e th levitation bogie and car body, which are given by

$$w_n = (y_e + q_e(-1)^n L_0) - (y_c - \theta_c L_n) \quad (16)$$

where L_n is the distance from the e th levitation bogie to the center of the car body.

The dynamic equilibrium equation of the car body can be expressed as

$$\begin{cases} M_c \ddot{y}_c - \sum_{n=1}^8 (k_s w_n + c_s \dot{w}_n) = 0 \\ J_c \ddot{\theta}_c + \sum_{n=1}^8 (k_s w_n + c_s \dot{w}_n) L_n = 0 \end{cases} \quad (17)$$

where J_c is the moment of inertia of the car body.

For the reliability of the maglev system, the control strategy of multi-point and independent suspension control has been applied to the high-speed maglev vehicle, in which the vehicle is mechanically decoupling and single-magnet suspension control system is adopted as the basic unit of the electromagnetic levitation controller. The controlled electromagnetic interaction force between the n th magnet and guideway can be written as (Shi and Wang 2011, Sinha 1987)

$$F_{mn} = K_0 \left(\frac{i_n}{h_n} \right)^2, \quad n = 1, 2, \dots, 8 \quad (18)$$

where i_n is the control current for the n th magnet, h_n is the levitation gap between n th magnet and guideway, which can be given as

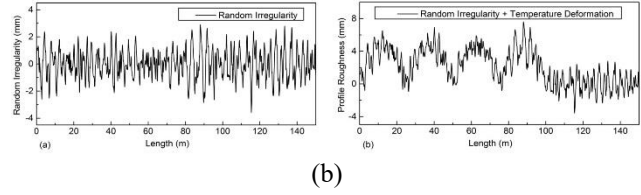
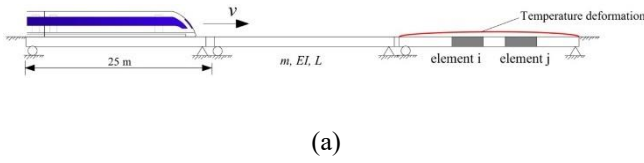


Fig. 13(a) Guideway random irregularity samples and (b) profile roughness samples

$$h_n = z_n - u_n - z_m - z_m \quad (19)$$

where u_n , z_m and z_m are the displacement, irregularity and temperature deformation of the guideway at the action position of the n th electromagnetic force, respectively. It is noted that a variation of the temperature deformation will induce a change of the levitation gap and electromagnetic interaction force, and then will influence the vibration of the maglev system. K_0 denotes the coupling factor, and can be obtained by the equation of the static equilibrium condition, i.e., $\ddot{y}_c = \ddot{\theta}_c = \ddot{y}_e = \ddot{q}_e = \ddot{z}_n = 0$ for the vehicle model, which is written as

$$K_0 \left(\frac{i_0}{h_0} \right)^2 = p_0 \quad (20)$$

where (i_0, h_0) is the desired values of control current and levitation gap around a specified nominal operating point for a maglev train model.

Based on references (Kim *et al.* 2015, Kong *et al.* 2011, Sinha 1987), a reasonably accurate linear model may be obtained by using linear approximations of the electromagnetic force for excursions around the nominal static equilibrium point (i_0, h_0) . In this study, the linearized electromagnetic force for the n th magnet is used and given as

$$F_{mn} = p_0 + C_i \Delta i_n - C_h \Delta h_n, \quad n = 1, 2, \dots, 8 \quad (21)$$

where $\Delta i_n = i_n - i_0$, $\Delta h_n = h_n - h_0$, $C_i = \left. \frac{\partial F_{mn}}{\partial i_n} \right|_{i_n=i_0, h_n=h_0} = \frac{2K_0 i_0}{h_0^2}$, $C_h = - \left. \frac{\partial F_{mn}}{\partial h_n} \right|_{i_n=i_0, h_n=h_0} = \frac{2K_0 i_0^2}{h_0^3}$.

The current control laws for the n th magnet can be given as (Goodall 2000, Shi and Wang 2011)

$$\Delta i_n = k_h \Delta h_n + k_v \dot{z}_n + k_a \ddot{z}_n, \quad n = 1, 2, \dots, 8 \quad (22)$$

where k_h , k_v and k_a are the feedback control gains related to the levitation gap change, the velocity and the acceleration of the magnet, and they can be determined by the transient-response characteristics of a controlled magnet (Ogata 2010).

Substituting Eqs. (21) and (22) into (13), one can achieve the following differential equation for the n th magnet

$$\begin{aligned} & (m + C_i k_a) \ddot{z}_n + (c_p + C_i k_v) \dot{z}_n + (k_p - C_h + C_i k_h) z_n \\ & - c_p \dot{y}_e - k_p y_e - (-1)^n L_0 c_p \dot{q}_e - (-1)^n L_0 k_p q_e \\ & = (C_i k_h - C_h) (h_0 + u_n + z_m) \end{aligned} \quad (23)$$

Combining Eqs. (15), (17) and (23) yields the following matrix equation of motion for the 18-DOF vehicle

$$[M_v] \{\ddot{u}_v\} + [C_v] \{\dot{u}_v\} + [K_v] \{u_v\} = \{P_v\} \quad (24)$$

where $[M_v]$, $[C_v]$, and $[K_v]$ are the mass, damping and stiffness matrices of the vehicle, respectively, $\{u_v\}$ represents the vertical displacement vector of the vehicle, $\{u_v\} = \{z_1; \dots; z_8; y_1; q_1; \dots; y_4; q_4; y_c; \theta_c\}$, $\{P_v\}$ is the load vector of the vehicle.

The parameters of the maglev vehicle are listed in Table 3, which are mainly based on the technical data of the maglev train running in Shanghai High-speed Maglev Commercial Operational Line.

4.2 Guideway subsystem

The guideway subsystem here is established using Finite Element Method (FEM) and simulated as beam elements since its span-to-width ratio is large enough. Compared to the widely used Mode Superposition Method, FEM can take into account all modal shapes and frequencies and consider more structural details and more complicated boundary conditions. Fig. 12 shows the guideway model considered as a series of simply supported beams. Then, the equation of motion for the guideway subsystem can be formulated as (Yang *et al.* 2004)

$$[M_g] \{\ddot{y}_g\} + [C_g] \{\dot{y}_g\} + [K_g] \{y_g\} = \{P_g\} \quad (25)$$

where $[M_g]$, $[C_g]$ and $[K_g]$ are the mass, damping and stiffness matrices of the guideway, $\{y_g\}$ represents all the nodal DOFs of the guideway, $\{P_g\}$ is the load vector of the guideway, which is given as

$$\{P_g\} = \sum_{n=1}^8 [\Gamma_n] \{N_{cn}\} F_{mn} \quad (26)$$

where F_{mn} is the n th electromagnetic force acting on the guideway, which can be obtained by Eqs. (18) and (19). $\{N_{cn}\}$ the displacement interpolation vector of the guideway element, the subscript cn indicates that the interpolation vector $\{N_{cn}\}$ is evaluated at the contact point of the n th electromagnetic force, $[\Gamma_n]$ is the coordinate transformation matrix which transforms the load $\{N_{cn}\} F_{mn}$ from the element vectors to the whole structural vectors. Rayleigh damping is assumed for the guideway, which means that the damping matrix of the entire guideway can be computed as a linear combination of the mass and stiffness matrices of the structure.

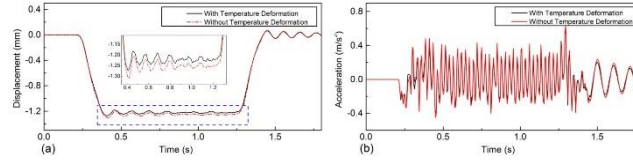


Fig. 14 Dynamic displacement and acceleration responses of the mid-span guideway

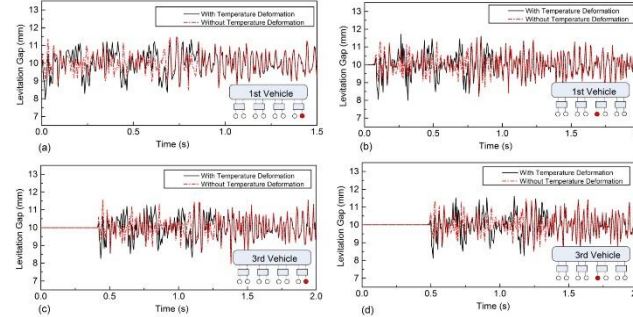


Fig. 15 Levitation gap variations histories for the first and middle magnets of the first and middle vehicles

4.3 Temperature deformation and guideway irregularity

In the analysis of maglev train/guideway interaction, both guideway irregularity and thermal deformation are used as the system excitation.

The time of a maglev train passing a guideway is rather short (only a few seconds), so the temperature deformation varying with time can be treated as a static profile roughness which is applied to the surface of guideways. The maximum vertical temperature deformation (shown in Fig. 9) at 16:00 induced by the solar radiation of the extreme condition is taken as the worst situation for the dynamic response investigation. The length of a guideway is 25 m, then the integral guideway deformations caused by temperature effect accordingly produce a series of the excitation in a wavelength range of 25 m. Therefore, the external excitations under temperature effect contain more components of the long wave.

To simulate the vertical profile of the guideway geometry variations, the random irregularity described by Power Spectral Density (PSD) was generally used (Ren *et al.* 2010, Shi *et al.* 2007, Talukdar and Talukdar 2016, Zhao and Zhai 2002). The random irregularity sample is generated from the track spectra proposed by the U.S. Federal Railroad Administration (FRA) with Class 6 (Yang *et al.* 2004), which is expressed as

$$S_v(\Omega) = \frac{kA_v\Omega_c^2}{\Omega^2(\Omega^2 + \Omega_c^2)} \quad (27)$$

where $S_v(\Omega)$ is vertical irregularities, with the units being $\text{cm}^2/(\text{rad}/\text{m})$, Ω (rad/m) is the spatial frequency, k is a dimensionless parameter and assumed 0.25 herein, $\Omega_c = 0.8245$ (rad/m) is the cut-off frequencies, $A_v = 3.39 \times 10^{-7}$ ($\text{m}^2 \cdot \text{rad}/\text{m}$) is the surface roughness constants, the wavelength is 0.5-50 m. The guideway profile roughness samples used in this study, including the irregularity samples and temperature deformation, are demonstrated in Fig. 13.

4.4 Numerical solution for the maglev/guideway interaction

With the Eqs. (23) and (24), the coupled motion equation for train/guideway system can be written as

$$\begin{bmatrix} M_v & 0 \\ 0 & M_g \end{bmatrix} \begin{Bmatrix} \ddot{u}_v \\ \ddot{u}_g \end{Bmatrix} + \begin{bmatrix} C_v & 0 \\ 0 & C_g \end{bmatrix} \begin{Bmatrix} \dot{u}_v \\ \dot{u}_g \end{Bmatrix} + \begin{bmatrix} K_v & 0 \\ 0 & K_g \end{bmatrix} \begin{Bmatrix} u_v \\ u_g \end{Bmatrix} = \begin{Bmatrix} P_v \\ P_g \end{Bmatrix} \quad (28)$$

Because of motion-dependent electromagnetic interactive forces, incremental-iterative method is used to solve the nonlinear dynamic analysis of the maglev vehicle/guideway system. More detailed information about the incremental-iterative procedure for dynamic analysis of maglev vehicle/guideway interaction is available in the references (Shi and Wang 2011, Yau 2009a). At this study, it is assumed that a maglev train consisting of five vehicles passes four consecutive same spans of the simply supported guideway at a constant speed of 430 km/h, which is the current maximum running speed for the maglev train in Shanghai Commercial Operational Line.

5. Numerical response analysis

5.1 The dynamic responses induced by temperature deformation

The previous thermal analysis revealed that the guideway deformation induced solar radiation reached its maximum at 16:00 of a sunny day in July. To illustrate the temperature effect on dynamic response, this temperature deformation is taken as the extreme situation to compare with a scenario with no temperature deformation.

Fig. 14 presents the dynamic displacement and acceleration of the mid-span guideway with and without temperature deformation. The comparison between the

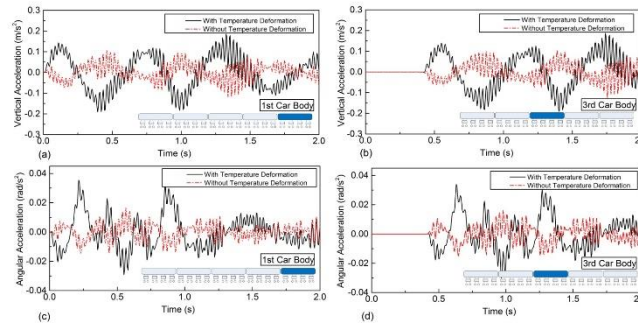


Fig. 16 Vertical and angular accelerations of the first and middle car bodies

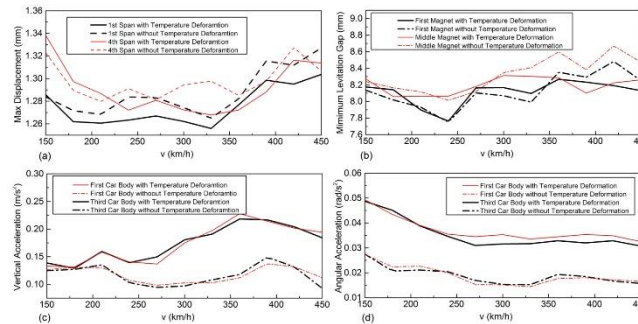


Fig. 17 Dynamic responses of the maglev system versus the train speed

responses with and without temperature deformation reveals that the upward camber temperature deformation results in an obvious reduction of the dynamic displacement while it has a weak influence on the acceleration response. In Fig. 14(a), at the train speed of 430 km/h and 4.72 mm maximum temperature deformation, the maximum dynamic displacement decreases from 1.31 mm to 1.27 mm corresponding to a 3.15% reduction. From Fig. 14(b), it can be found that there is little difference between the acceleration curves with and without temperature deformation. The reason for this phenomenon is that the deformation induced by temperature is a low-frequency excitation. For a guideway structure, dynamic displacements are mainly controlled by low-frequency excitations, and dynamic accelerations are dominated by high-frequency excitations.

Fig. 15 shows the levitation gap variations due to temperature deformation for the 1st magnet and middle magnet (4th magnet) of the 1st vehicle and those of the middle vehicle (3rd vehicle). It can be found that the temperature deformation significantly amplifies the variation of levitation gap, even doubles the variation at some points. This will lead to a higher demand for levitation stability control.

Fig. 16 shows the variations of vertical and angular accelerations due to temperature deformation for the 1st car body and middle car body (3rd car body). By comparison, it can be found that because of the upward camber temperature deformation, the vertical and angular accelerations are greatly enhanced. The maximum value of the vertical acceleration increases from 0.12 m/s² to 0.191 m/s² (59.2% rise), and the maximum value of the angular acceleration increases from 0.017 rad/s² to 0.036 rad/s² (111.8% rise). This will cause a low-quality ride for the

maglev train.

In addition, because the direction of thermal deformation is upward which is opposite to that of dynamic deformation, the change trend of the levitation gap and car body acceleration are opposite among these responses with and without temperature deformation.

5.2 The temperature effect with different train speeds

The effect of temperature deformation on dynamic responses may be different when the high-speed maglev train passes the guideway at different speeds. To investigate the temperature effect at various speeds, the dynamic responses of maglev train/guideway are calculated at the range of [150, 450] km/h. Fig. 17 exhibits the maximum dynamic responses varying with the train speed, which include the dynamic displacements, levitation gaps, and car body accelerations. It can be observed in Fig. 17(a) and (d) that, at different train speeds, the variations of dynamic displacement remain within 0.02 mm and the variations of angular acceleration remain approximately 0.02 rad/s². These small changes suggest that the temperature effects on displacement and angular acceleration are not significantly affected by train speed.

However, for the levitation gap and vertical acceleration, the temperature effects are greatly amplified when the speed rises from a low speed to a high speed. From the Fig. 17(b) and (c), it can be found that the variation of levitation gaps increases from 0.03 mm to 0.45 mm and the variation of vertical acceleration increase from 0.01 m/s² to 0.12 m/s² when the speed increases from 150 km/h to 450 km/h.

In Fig. 17(c), the vertical accelerations of car bodies are found to reach their amplitudes at the speeds of 360 km/h (with temperature deformation) and 390 km/h (without

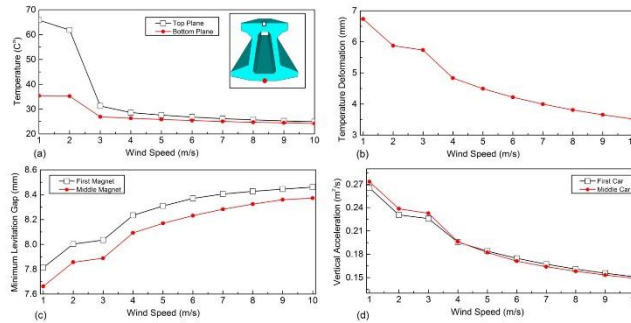


Fig. 18 The effect of wind speed on dynamic responses of the maglev system

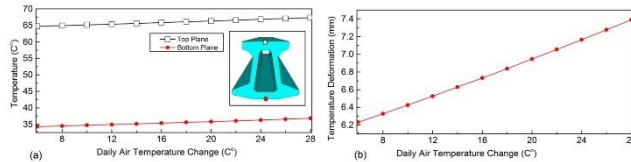


Fig. 19 The effect of ambient temperature change on dynamic responses of the maglev system

temperature deformation). According to the reference (Yang *et al.* 2004), the second resonance speed is computed at 387 km/h. When the train speed is near to the second resonance speed, the vibrations of maglev vehicles are amplified and the acceleration amplitudes are induced due to the effect of resonance. The difference of the resonance speeds with and without temperature deformation indicates that the temperature deformation may affect the resonance condition of the maglev system.

To sum up, the temperature effects on dynamic responses of maglev/guideway system are generally amplified with the increasing of the train speed, especially for the effects on levitation gap and vertical acceleration of car body.

5.3 Parametric study

The temperature field and deformation field of the guideway are highly related to the environmental conditions and the material of the guideway. Accordingly, the temperature effects on the dynamic responses of the maglev train/guideway system are also significantly affected by these factors. In this section, the influences of some environmental and material parameters on the critical performances of the maglev system are investigated.

5.3.1 Effect of wind speed

The wind speed affects the convection heat transfer coefficient (h_c), and then changes the temperatures of the guideway surfaces. Fig. 18 illustrates the effect of wind speeds on the performances at the wind speed range of 1 m/s to 12 m/s corresponding to weak and strong winds. It can be seen that the higher wind speeds tend to bring the temperature of the guideway surfaces closer to that of the ambient environment, which is more obvious for the top plane of guideway surfaces. It can also be found that with the increase of the wind speed, the maximum temperature deformation of the guideway decreases. Consequently, the increase of the wind speed leads to an obvious increase of the minimum levitation gaps, and a significant reduction of

the vertical acceleration of car bodies. These results indicate that the worst situation for the temperature distribution and dynamic performance occurs when the wind speed is equal to zero.

5.3.2 Effect of daily ambient temperature changes

The change of the ambient temperature results in a variation of the initial temperature of the guideway and a variation of the radiation heat transfer coefficient (h_r) between the guideways and the surrounding atmosphere, and then it affects the temperature field of the guideway and dynamic performance of the system. Fig. 19 presents the effect of daily ambient temperature changes on the temperatures of top and bottom planes and the thermal deformation at the temperature variation range of 6°C to 28°C. It can be seen that increasing the daily range increases both the temperature values and the deformations, but the increase is not very obvious. For example, for the maximum variation range of 28°C, the temperature variations of top and bottom planes are within 3°C and the deformation variation is less than 1 mm. As a result, the effect of ambient temperature range is even smaller on the dynamic performances of the maglev system.

5.3.3 Effect of thermal conductivity coefficient

Thermal conductivity coefficient (k) is a very important thermal coefficient for the concrete guideway, which is highly affected by the mineralogical characteristics of the concrete aggregate. In this study, the adopted range of the thermal conductivity coefficient is between 0.8 (W/(m·°C)) and 2.4 (W/(m·°C)). Fig. 20 shows the effect of thermal conductivity coefficient (k). It can be seen that the temperatures of the top and bottom plane reduce with the increase of the k , and this phenomenon is more obvious for the top plane. The temperature deformation increases as the k increases, but the increase of the deformation is not very significant. It can be observed that with the k rising from the lower bound to upper bound, the added deformation is less than 1 mm. Consequently, the effect of thermal conductivity coefficient is also weak on the dynamic performance of the

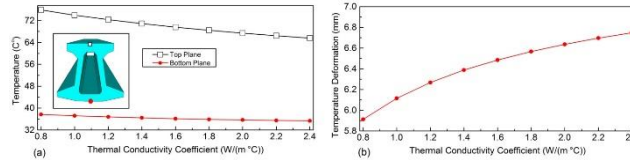


Fig. 20 The effect of thermal conductivity coefficient on dynamic responses of the maglev system

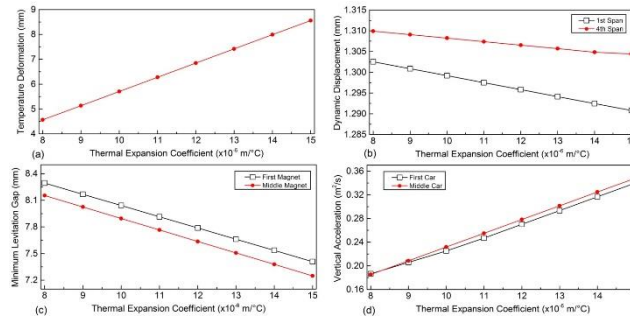


Fig. 21 The effect of thermal expansion coefficient on dynamic responses of the maglev system

maglev system.

5.3.4 Effect of thermal expansion coefficient

The thermal expansion coefficient (α_T) has little influence on the temperature distribution, but it has a strong influence on the stress field and thermal deformation. The effects of α_T on the performance of the maglev system are illustrated in Fig. 21 with the parameter range between 8×10^{-6} (m/°C) and 1.5×10^{-5} (m/°C). It can be found that the responses, including temperature deformation, dynamic displacement, minimum levitation gap and vertical acceleration, exhibit a linear change with a change in thermal expansion coefficient. The increase of the α_T causes a reduction of the minimum levitation gap and a rise of the vertical acceleration of car bodies, which poses a negative effect on the stability of levitation control and ride comfort of the maglev train.

6. Conclusions

This article presents a numerical analysis method to evaluate dynamic responses of the maglev train/guideway interaction system induced by deformation of the guideway subjected to climatic temperature changes, in which the whole process of solar radiation and heat exchange between guideways and environment was simulated based on the practical atmospheric conditions. Moreover, a parametric analysis has been conducted to investigate the temperature effects of various parameters, including train speeds, material properties, and climatic conditions, parameters, on the dynamic performances of the maglev train/guideway system. The following conclusions can be drawn:

- The proposed numerical analysis is effective to investigate the thermal responses of guideways. The effect of the time-varying shadow is simulated by an appropriate element mesh to the guideway model, the errors caused by the initial uniform temperature assumption for guideways are eliminated by running the thermal analysis through several cycling periods, and the solar radiation intensity

adopted for the thermal analysis is defined based on the local meteorological record or thermal design code. Therefore, in comparison to the generally used temperature load or temperature gradient load method, the analysis method in this article can precisely quantify and analyze the time-varying temperature field and deformation field of maglev guideways. This leads to a more reliable evaluation of temperature effect on the dynamic responses of the maglev train/guideway coupled system.

- The effect of temperature deformation on dynamic responses of the maglev system can be investigated by the proposed numerical train/guideway system. The thermal deformation, which acts as a low-frequency component of the irregularity excitations, brings an apparent influence on dynamic responses of the maglev train/guideway system. It causes a reduction of dynamic displacement of the guideway, and lead to a corresponding decrease of the minimum levitation gaps and an increase of vertical and angular accelerations of the car bodies. These effects induced by thermal deformation will result in a higher demand for levitation control and a low-quality ride for the maglev train.

- The increase of the train speed will generally amplify the temperature deformation effect on the dynamic responses of the maglev system, especially for the effects on the levitation gap and the vertical acceleration of the car body. Therefore, when the train speed rises up to a higher level, it is vital to control the thermal deformation of guideways to maintain the standard-compliant levitation stability and satisfactory ride comfort.

- Climatological conditions and thermal properties of concrete, which vary with the location, season and material of guideways, have a significant effect on the responses of the maglev system. Lower wind speed tends to induce a larger temperature difference between the top plane and bottom plane and a larger temperature deformation, and then it leads to a lower quality of levitation control and ride comfort. The increase of the daily ambient temperature range and thermal conductivity coefficient will result in an increase of the temperature difference and temperature

deformation, but their effects are not very significant under the present conditions. Their influences are weak on the dynamic performances of the maglev system. The increase of the thermal expansion coefficient obviously causes a reduction of the levitation gap and a rise of the vertical acceleration. Therefore, in order to achieve satisfactory performance of the maglev system, severe guideway structure design process particularly requires a thorough consideration of climatic loads and thermal properties of the material.

This study provides a reliable numerical calculation procedure to investigate the performance of the maglev train/guideway system under temperature effect. It may replace long-term testing of prototype guideway girders, which can save economical cost for the design and research of guideways. Moreover, the research results in this paper may be useful for the similar or further design of the maglev guideway. In addition, the proposed maglev train/guideway interaction model can be used for other related or further studies, for example, the response study under seismic excitations, and the simulation of the maglev train/guideway/tunnel interaction system.

Acknowledgments

This work is sponsored by the National 13th Five-Year Science and Technology Support Program of China (Project No: 2016YFB1200602).

References

- Branco, F.A., Mendes, P.A., Aguado, A. and Mirambell, E. (1991), "Design temperature differences for concrete bridges", *Struct. Eng. Int.*, **1**(3).
- Branco, F.A., Mendes, P.A. and Mirambell, E. (1992), "Heat of hydration effects in concrete structures", *ACI Mater. J.*, **89**(2), 139-145.
- Cai, Y. and Chen, S.S. (1996), "Vehicle/guideway dynamic interaction in Maglev systems", *J. Dyn. Syst. Measure. Contr.*, **118**, 526-530.
- Cai, Y., Chen, S.S., Rote, D.M. and Coffey, H.T. (1994), "Vehicle/guideway interaction for high speed vehicles on a flexible guideway", *J. Sound Vibr.*, **175**(5), 625-646.
- GB 50176-93 (1993), *Thermal Design Code for Civil Building*, Department of Construction of the PRC, Beijing, China.
- Goodall, R.M. (2000), "On the robustness of flux feedback control for electro-magnetic Maglev controller", *Proceedings of the 16th International Conference on Magnetically-Levitated Systems and Linear Drives*.
- Han, J.B., Han, H.S., Kim, S.S., Yang, S.J. and Kim, K.J. (2016), "Design and validation of a slender guideway for Maglev vehicle by simulation and experiment", *Vehic. Syst. Dyn.*, **54**(3), 370-385.
- Huang, J.Y., Wu, Z.W., Gao, Y. and Wang, D.Z. (2018), "Influence of track irregularities in high-speed Maglev transportation systems", *Smart Struct. Syst.*, **21**(5), 571-582.
- Ju, S.H., Leong, C.C. and Ho, Y.S. (2014), "Safety of maglev trains moving on bridges subject to foundation settlements and earthquakes", *J. Brid. Eng.*, **19**(1), 91-100.
- Kim, K.J., Han, J.B., Han, H.S. and Yang, S.J. (2015), "Coupled vibration analysis of Maglev vehicle-guideway while standing still or moving at low speeds", *Vehic. Syst. Dyn.*, **53**(4), 587-601.
- Kong, E., Song, J.S., Kang, B.B. and Na, S. (2011), "Dynamic response and robust control of coupled maglev vehicle and guideway system", *J. Sound Vibr.*, **330**(25), 6237-6253.
- Lee, J.S., Kwon, S.D., Kim, M.Y. and Yeo, I.H. (2009), "A parametric study on the dynamics of urban transit maglev vehicle running on flexible guideway bridges", *J. Sound Vibr.*, **328**(3), 301-317.
- Liu, H., Chen, Z. and Zhou, T. (2012), "Numerical and experimental investigation on the temperature distribution of steel tubes under solar radiation", *Struct. Eng. Mech.*, **43**(6), 1-13.
- Mamdouh, M.E. and Amin, G. (1984), "Temperature variations in concrete bridges", *J. Struct. Eng.*, **110**(12), 3059-3060.
- Mangerig, I., Zapfe, C., Lichte, U. and Zapf, O. (2005), *Thermal Effects on Guideways for High Speed Magnetic Levitation Transportation Systems*, Unpublished Work.
- Min, D.J., Jung, M.R., Kim, M.Y. and Kwark, J.W. (2017a), "Dynamic interaction analysis of Maglev-guideway system based on a 3D full vehicle model", *Int. J. Struct. Stab. Dyn.*, **17**(1), 1750006.
- Min, D.J., Lee, J.S. and Kim, M.Y. (2012), "Dynamic interaction analysis of actively controlled maglev vehicles and guideway girders considering nonlinear electromagnetic forces", *Coupled Syst. Mech.*, **1**(1), 39-57.
- Min, D.J., Kwon, S.D., Kwark, J.W. and Kim, M.Y. (2017b), "Gust wind effects on stability and ride quality of actively controlled maglev guideway systems", *Shock Vibr.*
- Ogata, K. (2010), *Modern Control Engineering*, Prentice Hall.
- Ren, S., Romeijn, A. and Klap, K. (2010), "Dynamic simulation of the Maglev vehicle/guideway system", *J. Brid. Eng.*, **15**(3), 269-278.
- Shi, J. and Wang, Y.J. (2011), "Dynamic response analysis of single-span guideway caused by high speed maglev train", *Lat. Am. J. Sol. Struct.*, **8**, 1-14.
- Shi, J., Wei, Q. and Zhao, Y. (2007), "Analysis of dynamic response of the high-speed EMS maglev vehicle/guideway coupling system with random irregularity", *Vehic. Syst. Dyn.*, **45**(12), 1077-1095.
- Sinha, P.K. (1987), *Electromagnetic Suspension Dynamics & Control*, Magnetic Levitation Vehicles.
- Song, M.K. and Fujino, Y. (2008), "Dynamic analysis of guideway structures by considering ultra high-speed Maglev train-guideway interaction", *Struct. Eng. Mech.*, **29**(4), 355-380.
- Talukdar, R.P. and Talukdar, S. (2016), "Dynamic analysis of high-speed Maglev vehicle-guideway system: An approach in block diagram environment", *Urb. Rail Transit*, **2**(2), 71-84.
- TB10002.3 (2005), *Code for Design Reinforced and Prestressed Concrete Structure of Railway Bridge and Culvert*, China Railway Publishing House, Beijing, China.
- Tian, Y., Zhang, N. and Xia, H. (2017), "Temperature effect on service performance of high-speed railway concrete bridges", *Adv. Struct. Eng.*, **20**(6), 865-883.
- Walter, H.D., Amin, G., Mathew, C., Mo, C.S. and Marc, M.A. (1983), "Temperature stresses in composite box girder bridges", *J. Struct. Eng.*, **109**(6), 1460-1478.
- Wu, X. and Huang, J. (2004), "Guideway structure, Maglev demonstration line, Shanghai", *J. Int. Assoc. Brid. Struct. Eng.*, **14**(1), 21-23.
- Yang, Y.B. and Yau, J.D. (2011), "An iterative interacting method for dynamic analysis of the maglev train-guideway/foundation-soil system", *Eng. Struct.*, **33**(3), 1013-1024.
- Yang, Y.B., Yau, J.D. and Wu, Y.S. (2004), *Vehicle-Bridge Interaction Dynamics with Application to High Speed Railways*, World Scientific Publishing Co. Pte. Ltd, Singapore.
- Yau, J.D. (2009a), "Vibration control of maglev vehicles traveling

- over a flexible guideway”, *J. Sound Vibr.*, **321**(1-2), 184-200.
- Yau, J.D. (2009b), “Response of a maglev vehicle moving on a series of guideways with differential settlement”, *J. Sound Vibration*, **324**(3–5), 816–831.
- Yau, J.D. (2010a), “Response of a Maglev vehicle moving on a two-span flexible guideway”, *J. Mech.*, **26**(1), 95-103.
- Yau, J.D. (2010b), “Aerodynamic vibrations of a maglev vehicle running on flexible guideways under oncoming wind actions”, *J. Sound Vibr.*, **329**(10), 1743-1759.
- Yau, J.D. (2010c), “Interaction response of maglev masses moving on a suspended beam shaken by horizontal ground motion”, *J. Sound Vibr.*, **329**(2), 171-188.
- Yau, J.D. (2013), “Wave passage effects on the seismic response of a maglev vehicle moving on multi-span guideway”, *Lat. Am. Sol. Struct.*, **10**(5), 981-1000.
- Zhang, L. and Huang, J. (2018), “Stiffness of coupling connection and bearing support for high-speed Maglev guideways”, *J. Brid. Eng.*, **23**(9).
- Zhao, C. and Zhai, W. (2002), “Maglev vehicle/guideway vertical random response and ride quality”, *Vehic. Syst. Dyn.*, **38**(3), 185-210.

CC